Swelling Kinetics of a Microgel Shell

Joshua Wahrmund,[†] Jin-Woong Kim,[‡,§] Liang-Yin Chu,[‡,||] Changjie Wang,[⊥] Yong Li,[#]
Alberto Fernandez-Nieves,[‡,▽] David A. Weitz,*,[‡] Arkadii Krokhin,*,[†] and Zhibing Hu*,[†]

[†]*Department of Physics, University of North Texas, Denton, Texas 76203,* [‡]*School of Engineering and Applied Sciences, Department of Physics, Harvard University, Cambridge, Massachusetts 02138,* [§]*Amore-Pacific R&D Center, 314-1, Bora-dong, Giheung-gu, Yongin-si, Gyeonggi-Do, 446-729 Korea,* [||]*School of Chemical Engineering, Sichuan University, Chengdu, Sichuan 610065, China,* [⊥]*Haynes and Boone, LLP, Richardson, Texas 75082,* [#]*Kimberly-Clark Corporation, Neenah, Wisconsin 54957, and* [▽]*School of Physics, Georgia Institute of Technology, Atlanta, Georgia 30332*

ABSTRACT: Tanaka's approach to swelling kinetics of a solid gel sphere is extended to a spherical microgel shell. The boundary condition at the inner surface is obtained from the minimization of shear elastic energy. Temporal evolution of a shell is represented in a form of expansion over eigenfunctions of the corresponding diffusion equation. The swelling of Tanaka's solid spherical gel is recovered as a special case of our general solution if the inner radius approaches zero. In another limiting case of a thin (balloon-like) shell, the set of eigenfunctions is reduced to a single exponential term. In the general case, a solid sphere swells slightly faster than the same sphere with an internal cavity. To test our theoretical model, we prepared monodisperse poly-*N*-isopropylacrylamide (PNIPAM) hydrogel shells using a microfluidic device. The temporal dependence of the inner and outer radii of the shell were measured, and the data were fitted to our theoretical model. As a result, we obtained the collective diffusion constants for shrinking and for swelling processes. The obtained values for microgel shells are in excellent agreement with the previous results obtained for submillimeter PNIPAM solid spheres in the same temperature interval. Our model shows that the characteristic swelling time of a gel shell should be proportional to the square of the outer radius not to the thickness of the shell, agreeing with experimental observation.

1. Introduction

Polymer gels have been studied extensively because of their ability to simulate biological tissues and to swell or collapse reversibly in response to external stimuli.[1−8] Swelling of polymer gels is one of the classical problems in both macromolecular science and technology.[9−12] Flory and Rehner developed an equilibrium swelling theory by considering the balance between the mixing of polymer chains with solvent and the elasticity of the polymer chains.[9] Ritger and Peppas presented mathematical models for drug diffusion from hydrogels.[10] Tanaka and Fillmore have studied the swelling kinetics of spherical gels[11] by using an equation of motion of the gel network.[12]

The study of swelling kinetics has been further extended to different geometries: long solid gel cylinders and thin solid disks.[13−15] In these cases, a theoretical analysis of the kinetics of gel swelling and solvent motion is based on the solution of coupled equations of motion for a network and solvent.[16] Urayama et al. studied the kinetics of shrinking for polymer gels induced by ultracentrifugal fields.[17] The swelling dynamics of a long solid cylindrical gel were analyzed by the stress diffusion coupling model, where the swelling is caused by an elongation force applied to the gel.[18] A continuum mechanical model was proposed for dynamical processes in swelling gels, in which solvent permeation causes deformation.[19] Furthermore, a model for transient deformation of neutral hydrogels that accounts for conservation of momentum, energy, and mass for the solid polymer and fluid phase was derived.[20]

Most of these previous theoretical studies have focused on the swelling kinetics for solid gel structures, that is, structures without internal cavities. The theory of gel shells is still missing. At the same time, experimental work on hollow polymer gels is making rapid progress. For example, a positively thermosensitive drug-release microcapsule was designed, and its preparation was carried out by the use of an air suspension coating technique for controlled drug release.[21] Mammalian cells were encapsulated in cylindrical hydrogel microstructures or in cubic hydrogel structures in microfluidic channels.[22] Submicrometer hydrogel cages have been prepared as drug carriers.[23] Hollow capsules composed of microgel particles have been synthesized with the microgel particles assembling on the surfaces of water droplets in oil.[24]

What actually motivates this work is the current synthesis of monodisperse polymer gel shells by microfluidic devices.[25,26] These gel shells have radii of ∼60 μm and have characteristic swelling times that range around several tens of seconds. The kinetics of these shells is easily measurable, but there is a lack of theoretical description. The study of the swelling kinetics of gels with shell structure will not only enhance our deep-seated understanding of swelling kinetics for polymer networks but may also aid in the development of applications ranging from controlled drug release to cell encapsulations.

Here we propose a theoretical model of swelling kinetics for a polymer gel shell.

This work is an extension of Tanaka's work on a solid gel to a shell gel. Just as with Tanaka's formulation for a solid gel, our model for a gel shell is based on the motion of the gel network. In each case, the motion of the gel network is determined by considering the mechanical stress within the gel network. The

Corresponding authors. zbhu@unt.edu (Z.H.); arkady@unt.edu (A.K.); weitz@seas.harvard.edu (D.A.W.).

solution for a solid sphere requires a single boundary condition at the outer surface. Usually, this is a stress-free boundary condition. For a shell with an internal cavity, one has to formulate the boundary condition at the inner surface as well. Assuming that swelling is a slow process with instantaneous relaxation of any mechanical fluctuations leading to the increase in shear elastic energy, the principle of minimization of shear energy can be formulated in a general form.[15] The missing boundary condition at the inner surface can be obtained from this principle. Because this new boundary condition breaks the Hermiticity of the eigenvalue problem for the diffusion equation, the solution of this equation is expanded over a nonorthogonal set of eigenfunctions. As a result, the Gram-Schmidt orthogonalization procedure is a necessary step on the way to the final solution. To test this solution, we have prepared thermally responsive poly-N-isopropylacrylamide (PNIPAM) shells using the microfluidic method. Experimental data fit well with the proposed theoretical model and also lead to values of the diffusion constant that are close to those known from previous experiments.

2. Theory

2a. Solid Sphere–Tanaka's Model. In the Tanaka et al. model[11] for a solid gel sphere, the kinetics of swelling is described by a vector $u(r,t)$. This vector is defined as the displacement of a point in the network from its equilibrium location r after the gel is fully swollen. That is, $u = 0$ at $t \to \infty$. Note that this concept is generalized as interchangeable with respect to the cases of both shrinking and swelling provided the conventions $u > 0$ (for shrinking) and $u < 0$ (for swelling), where u is one of the projections of the vector u. Newton's second law can be expressed as

$$\rho \frac{\partial^2 u}{\partial t^2} = \nabla \cdot \tilde{\sigma} - f \frac{\partial u}{\partial t} \qquad (1)$$

where ρ is the density of the medium, $\tilde{\sigma}$ is the stress tensor whose component σ_{ik} gives the force along the x_i direction on a unit plane perpendicular to the x_k axis, and f is the friction constant that reflects the drag force between a liquid and a gel. For a sphere in the steady stage of swelling when the acceleration is equal to zero, eq 1 reads

$$\frac{\partial u}{\partial t} = \hat{D}u, \quad (0 < r < a) \qquad (2)$$

where we have introduced $\hat{D}$, the diffusion operator in spherical coordinates

$$\hat{D} = D_0 \frac{d}{dr}\left(\frac{1}{r^2}\frac{d}{dr}(r^2 \ldots)\right) \qquad (3)$$

with $D_0 = (K + {}^4/_3\mu)/f$ being the collective diffusion constant of the gel network. K and μ are the bulk and shear moduli of the gel network, respectively. For Tanaka's gel sphere, a free surface boundary condition at $r = a$ is imposed. That is, there is no normal stress at the outer surface

$$\sigma_{rr} = \frac{K}{r^2}\left[\frac{\partial}{\partial r}(r^2 u)\right]\bigg|_{r=a} = 0 \qquad (4)$$

and at the origin the displacement is zero. The initial condition at $t = 0$ requires a uniform radial stress throughout the volume of the sphere. We can see from the left-hand side of eq 4 that a constant radial stress is easily satisfied with a linear deformation

$$u(r, t = 0) = -\Delta a \frac{r}{a} \qquad (5)$$

where a is the final radius of the gel sphere in equilibrium with the surrounding fluid, and Δa denotes the total increase in the radius of the sphere in the entire process of swelling, that is, $a - \Delta a$ is the radius of the sphere before swelling.

Using the initial and boundary conditions above, the solution of eq 2 is obtained in the form of an eigenfunction decomposition[11]

$$u(r,t) = -6\Delta a \sum_{n=1}^{\infty} \frac{(-1)^n}{\lambda_n a}\left[\frac{\lambda_n r \cos(\lambda_n r) - \sin(\lambda_n r)}{(\lambda_n r)^2}\right]e^{-D_0\lambda_n^2 t} \qquad (6)$$

where

$$\lambda_n = \frac{n\pi}{a} \qquad (7)$$

is the spectrum obtained from eq 4.

2b. Generalization of Tanaka's Model to Shell Geometry. *Boundary Conditions.* Here we consider the swelling of a shell with outer and inner radii a and b, respectively. For the outer layer, there is the same stress-free boundary eq 4. The boundary condition at the inner surface is obtained from the minimization of shear elastic energy. The total elastic energy of a gel can be separated into bulk and shear components. The bulk elastic energy of the gel is related to the volume change, which is controlled by the diffusion of the network. The shear elastic energy can be minimized by readjusting the shape of the gel without changing its volume. This means physically that although the shear modulus of the gel is much less than the bulk modulus and therefore can be neglected in the dynamical equation, the shear modulus still plays an important role preserving the shape of the gel.[15] For a shell, any change in diameter is coupled to a change in its thickness. The shear elastic energy for a gel of arbitrary shape is given by the following integral

$$F_{sh} = \mu \int_v \left(u_{ik} - \frac{1}{3}\delta_{ik}u_{ll}\right)^2 dV \qquad (8)$$

where we have adopted summation convention over the repeated indices i, k, l. The minimum of this functional is reached if the variation of the total shear elastic energy in response to any small change in shape, which maintains constant volume elements within the gel, vanishes, that is

$$\delta F_{sh} = 0 \qquad (9)$$

For a spherical shell, $u = (u,0,0)$ and the nonvanishing strain tensor components are given by $u_{rr} = \partial u/\partial r$, $u_{\theta\theta} = u_{\varphi\varphi} = u/r$. eq 8 then becomes

$$F_{sh} = 4\pi\mu\frac{2}{3}\int_b^a r^2\left(\frac{\partial u}{\partial r} - \frac{u}{r}\right)^2 dr \qquad (10)$$

This integral must be minimized. If the variations of the radii are δa and δb, then the variation of the volume is $\delta V = 4\pi(a^2\delta a - b^2\delta b)$. Because for shear deformations $\delta V = 0$,

we have the following from combining eqs 9 and 10

$$\delta F_{\text{sh}} = \frac{8}{3}\pi\mu\left[\int_{b+\delta b}^{a+\delta a} r^2\left(\frac{\partial u}{\partial r}-\frac{u}{r}\right)^2 dr - \int_b^a r^2\left(\frac{\partial u}{\partial r}-\frac{u}{r}\right)^2 dr\right]$$

$$= \frac{8}{3}\pi\mu\left[\left(\frac{\partial u}{\partial r}-\frac{u}{r}\right)^2\Big|_{r=a} - \left(\frac{\partial u}{\partial r}-\frac{u}{r}\right)^2\Big|_{r=b}\right] a^2\,\delta a = 0 \tag{11}$$

Because δa is an independent variation, the following boundary condition must be imposed

$$\frac{u(b,t)}{b} - \frac{\partial u(r,t)}{\partial r}\Big|_{r=b} = \frac{u(a,t)}{a} - \frac{\partial u(r,t)}{\partial r}\Big|_{r=a} \tag{12}$$

The solution of the diffusion eq 2 with the boundary conditions eqs 4 and 12 and the initial condition eq 5 defines the kinetics of swelling.

Solution of Diffusion Equation. A solution of the diffusion eq 2 satisfying the boundary condition eq 4 is written as a superposition of eigenfunctions

$$u(r,t) = \sum_{n=1}^{\infty} A_n Z_n(r)e^{-\lambda_n^2 D_0 t} \tag{13}$$

$$Z_n(r) = \frac{\cos[\lambda_n(r-a)]}{\lambda_n r} - \frac{\sin[\lambda_n(r-a)]}{(\lambda_n r)^2} \tag{14}$$

From the boundary condition at the inner surface (eq 12), we obtain

$$\frac{Z_n(b)}{b} - Z_n'(b) = \frac{Z_n(a)}{a} - Z_n'(a) \tag{15}$$

This relation gives the equation for the spectrum of the eigenvalues λ_n

$$3\cos[\lambda_n(a-b)] - (b^2\lambda_n^2 - 3)\frac{\sin[\lambda_n(a-b)]}{\lambda_n b} = 3\frac{b^2}{a^2} \tag{16}$$

The unknown coefficients A_n are calculated using the initial condition eq 5. For $t = 0$, we have from eqs 13 and 5

$$\frac{\Delta a}{a}r = \sum_{n=1}^{\infty} A_n Z_n(r) \tag{17}$$

The coefficients A_n cannot be directly calculated from this expansion because the eigenfunctions $Z_n(r)$ are not orthogonal. This comes from the fact that the boundary condition at $r = b$ breaks the Hermiticity of the diffusion operator

$$\hat{D} = D_0\frac{d}{dr}\left(\frac{1}{r^2}\frac{d}{dr}(r^2...)\right) \tag{18}$$

It is easy to show that the Hermiticity condition $\langle u,\hat{D}v\rangle = \langle v,\hat{D}u\rangle$ is not satisfied because of the nonzero boundary condition eq 12

$$\langle u,\hat{D}v\rangle = \langle v,\hat{D}u\rangle + D_0 v(b)\frac{d}{dr}(r^2 u)\Big|_{r=b} - D_0 u(b)\frac{d}{dr}(r^2 v)\Big|_{r=b} \tag{19}$$

Although the eigenfunctions $Z_n(r)$ of the non-Hermitian eigenvalue problem are not orthogonal

$$\langle Z_n, Z_m\rangle = \int_b^a r^2 Z_n(r)Z_m(r)\,dr$$

$$= \frac{\sin[\lambda_n(a-b)]\sin[\lambda_m(a-b)]}{b\lambda_m^2\lambda_n^2}$$

$$+ \frac{1}{\lambda_m\lambda_n(\lambda_m^2-\lambda_n^2)}\{\lambda_m\sin[\lambda_m(a-b)]\cos[\lambda_n(a-b)]$$

$$- \lambda_n\sin[\lambda_n(a-b)]\cos[\lambda_m(a-b)]\} \neq 0 \tag{20}$$

they are linearly independent because the corresponding Wronskian does not vanish

$$W(Z_n(r),Z_m(r)) = \begin{vmatrix} Z_n'(r), Z_m'(r) \\ Z_n(r), Z_m(r) \end{vmatrix} = Z_m Z_n' - Z_n Z_m'$$

$$= \frac{1}{r^2}\left\{\frac{1}{\lambda_n}\cos[\lambda_n(r-a)]\sin[\lambda_m(r-a)]\right.$$

$$\left. - \frac{1}{\lambda_m}\cos[\lambda_m(r-a)]\sin[\lambda_n(r-a)]\right\} \neq 0. \tag{21}$$

Therefore, the functions $Z_n(r)$ form a nonorthogonal basis, and the orthogonalization procedure is the necessary step.

Gram−Schmidt Orthogonalization Procedure. We apply the Gram−Schmidt orthogonalization procedure to form an orthonormal basis.[27] The ith vector of the orthonormal basis is calculated as follows

$$n_i(r) = \alpha_i\{Z_i(r) - \sum_{j=1}^{i-1}\langle Z_i|n_j\rangle n_j\} \tag{22}$$

$$\langle Z_i|n_j\rangle \equiv \int_b^a Z_i n_j r^2\,dr \tag{23}$$

Here the coefficients α_i are calculated from the normalization condition

$$\int_b^a n_i^2(r)r^2\,dr = \alpha_i^2\int_b^a r^2\{Z_i(x) - \sum_{j=1}^{i-1}\langle Z_i|n_j\rangle n_j\}^2\,dr = 1 \tag{24}$$

Therefore, each basis vector $n_i(r)$ is a linear combination of the vectors $Z_i(r)$. For example, $n_1 = \alpha_1 Z_1(r)$, $n_2 = \alpha_2\{Z_2(r) - \langle Z_2|n_1\rangle n_1\} = \alpha_2\{Z_2(r) - \langle Z_2|n_1\rangle\alpha_1 Z_1(r)\}$. Here we give the first three basis vectors

$$n_1(r) = \frac{Z_1(r)}{V_1}, \quad V_n^2 = \int_b^a r^2 Z_n^2(r)\,dr \tag{25}$$

$$n_2(r) = \frac{1}{V_1\sqrt{V_1^2 V_2^2 - \gamma_{12}^2}}\{V_1^2 Z_2(r) - \gamma_{12}Z_1(r)\} \tag{26}$$

$$n_3(r) = \frac{V_1^2 V_2^2 Z_3(r) - V_2^2\gamma_{13}Z_1(r) - V_1^2\gamma_{23}Z_2(r)}{V_1 V_2\sqrt{V_1^2 V_2^2 V_3^2 - V_2^2\gamma_{13}^2 - V_1^2\gamma_{23}^2}} \tag{27}$$

$$\gamma_{mn} = \int_b^a r^2 Z_m(r)Z_n(r)\,dr, \quad V_n^2 = \int_b^a r^2 Z_n^2(r)\,dr \tag{28}$$

Once we have calculated the (infinite) number of orthonormal vectors $n_i(r)$, we can expand the left hand side of eq 17 over the basis of $n_i(r)$

$$u(r, 0) = \frac{\Delta a}{a} r = \sum_{i=1}^{\infty} C_i n_i(r) \quad (29)$$

Now, owing to the orthonormality of the unit vectors $n_i(r)$, the coefficients C_i can be calculated in a standard form

$$C_i = \frac{\Delta a}{a} \int_b^a r^3 n_i(r) \, dr \quad (30)$$

Each $n_i(r)$ is a linear combination of eigenfunctions $Z_i(r)$. (See eq 22.) Substituting these linear combinations in eq 29, we can now calculate the unknown coefficients A_i by equating the coefficients of the $Z_i(r)$ on both sides of the following equation

$$\sum_{i=1}^{\infty} C_i n_i(r) = \sum_{i=1}^{\infty} A_i Z_i(r) \quad (31)$$

Once we know A_i, we can substitute them into the solution eq 13. Because in practice one can keep only a finite number of terms, the accuracy of the obtained solution increases with time, whereas the terms with larger λ_i are dying off exponentially.

Two Limiting Cases. Tanaka's solution for a solid gel becomes a special case of our shell model: as the inner radius
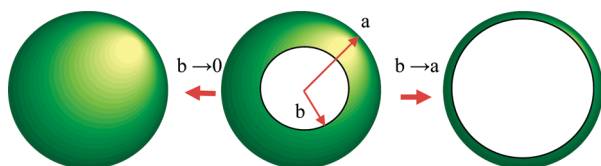

Figure 1. Scheme of the present model for spherical shell geometries. As the inner radius approaches zero, we retrieve Tanaka's solution for a solid sphere. In the opposing limit where the inner radius approaches the outer radius, the model describes a thin film "balloon".

$b \to 0$ (left panel in Figure 1), the general solution of a gel shell is reduced to Tanaka's solid sphere solution. This is easily demonstrated by first considering the eigenvalue spectrum eq 16. In the limit where b approaches zero, this equation reduces directly to the previous spectrum, eq 7. The eigenfunctions from eq 14 are then simplified considerably. Most importantly, the Hermiticity of the diffusion operator eq 3 is no longer broken, and so the eigenfunctions $Z_n(r)$ are orthogonal. They are given by the following formula

$$Z_n(r) = (-1)^n \left[\frac{\lambda_n r \cos \lambda_n r - \sin \lambda_n r}{(\lambda_n r)^2} \right] \quad (33)$$

With this set of eigenfunctions, the solution to Tanaka's sphere eq 6 is recovered by substitution of eq 33 into eq 13 with the implementation of the initial condition eq 5.

In the opposing limit, where the shell becomes very thin (i.e., $b \to a$, right panel in Figure 1), our solution reduces to a thin shell solution. Again, beginning with the eigenvalue spectrum from eq 16 and taking the limit where $a - b \ll b$, we obtain

$$\lambda = \frac{3}{a} \quad (34)$$

Therefore, the spectrum is reduced to a single eigenvalue. All higher order contributions over $(a - b)/b$ can be neglected in this limit as the separation between neighboring eigenvalues increases dramatically, that is, $\lambda_1 \ll \lambda_2 \ll \lambda_3 \ll \ldots$ With exponential accuracy, one can leave only the first term in eq 13 to obtain the solution for a balloon

$$u(r, t) \cong \Delta a e^{-9 D_0 t / a^2} \quad (35)$$

3. Experimental Section

3a. Synthesis of Microgel Shells. The microgel shells were synthesized using a capillary-based microfluidic device[25] that was made of three separate capillary tubes, as shown in Figure 2a. The two internal cylindrical tubes served as injection
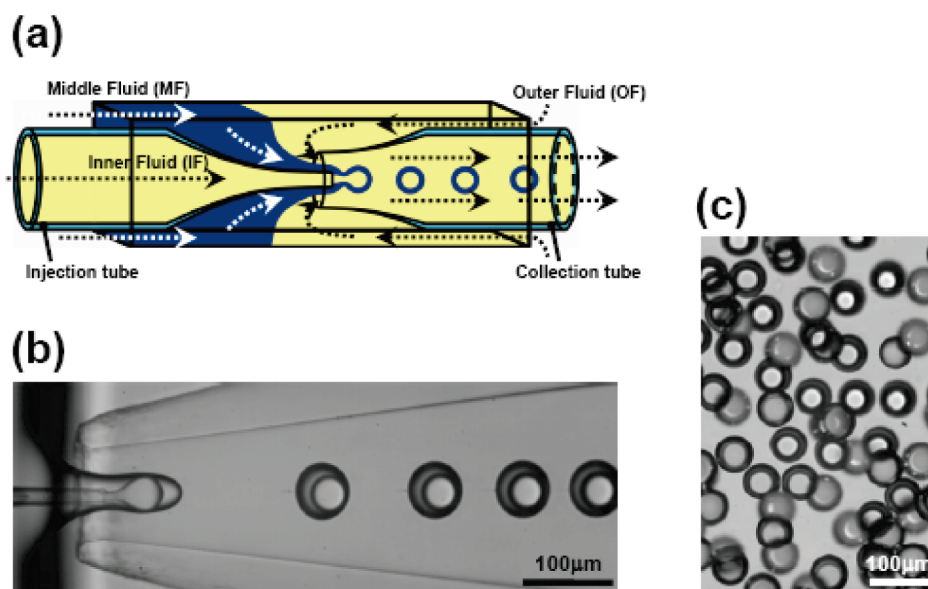

Figure 2. (a) Scheme for making premicrogel double emulsions in a capillary microfluidic device. (b) Formation of premicrogel double emulsion drops. These drops were prepared under the following flow conditions: $Q_{IF} = 100 \, \mu L \cdot h^{-1}$, $Q_{MF} = 300 \, \mu L \cdot h^{-1}$, and $Q_{OF} = 2000 \, \mu L \cdot h^{-1}$. (c) Uniform microgel shells formed after solidifying the emulsion by the redox reaction.
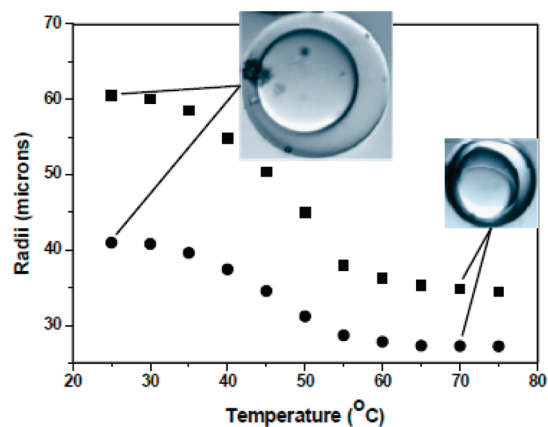
Figure 3. Temperature dependence of the inner (●) and outer (■) radii of the ionic microgel shell (batch 1). All swelling measurements were carried out in pure water.
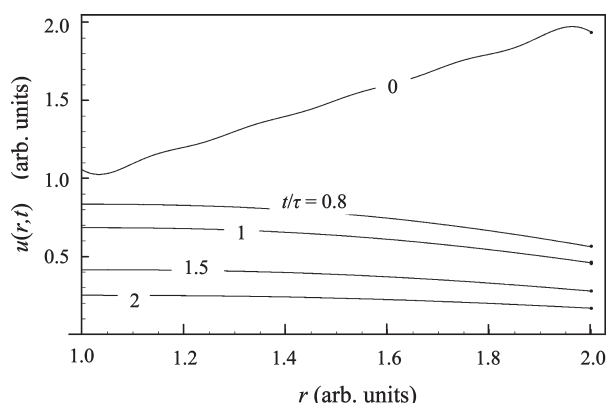

Figure 4. Displacement vector $u(r,t)$ is plotted as a function of r from b to a at different values of the scaled time t/τ. For these curves, the parameters are selected as $a = 2$, $b = 1$, and $\Delta a = 2$.
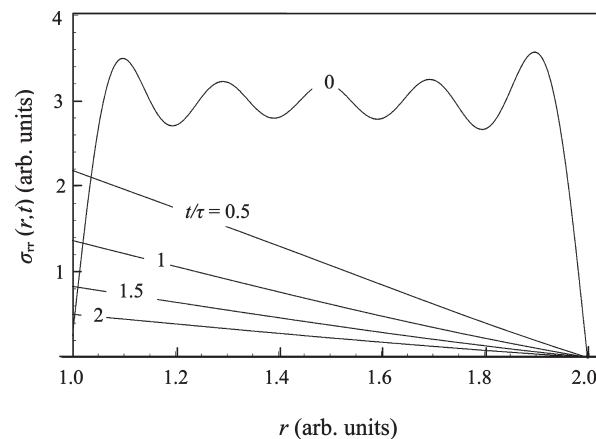

Figure 5. Radial stress tensor $\sigma_{rr}(r,t)$ is plotted as a function of r for different values of the scaled time t/τ. For this set of curves, we have set $a = 2$, $b = 1$, and $\Delta a = 2$.
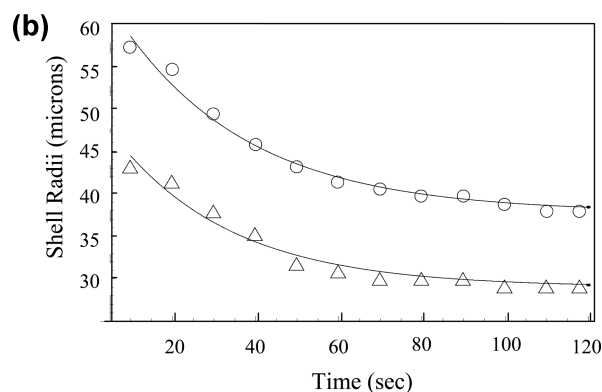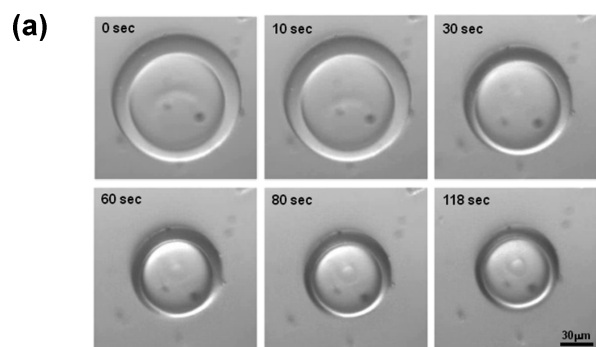
(a)

(b)

Figure 6. (a) Shrinking of the ionic gel shell (batch 1) was recorded with a digital camera with a time lapse of 1 s. A typical microgel shell was allowed to equilibrate at room temperature for 24 h. Then, he temperature of the sample was quickly raised from room temperature to 60 °C. (b) Plots of the experimental data as outer (○) and inner (△) radii, respectively. The solid curves are calculated using eq 36.

and collection tubes and were coaxially aligned. In the region near both tips, the outer fluid focused both the middle and inner fluids through the collection tube to form a fluid thread that then breaks into drops because of hydrodynamic instabilities. When generating the microgel shell structure, we used silicone oil (DC no. 550, density = 1.06 g·mL^{-1})) with viscosity η_{OF} = 125 mPa·s as the inner fluid, which was immiscible with the aqueous middle fluid. The inner fluid consisted of DC no. 550 and a reaction accelerator (N,N,N',N'-tetramethylethylenediamine, 2 vol %). The drops pinched-off to produce uniform double emulsions, where each aqueous premicrogel drop contained a single oil droplet. The outer fluid (OF) was DC no. 550. The middle fluid (MF) for the batch 1 sample was an aqueous monomer solution that contained the N-isopropylacrylamide (NIPAm, 15.5% w/v), a cross-linker (N,N'-methylenebisacrylamide, BIS, 1.5% w/v), two comonomers (2-(methacryloyloxy) ethyl trimethyl ammonium chloride (METAC, 2 vol %), allylamine (1 vol%)), and an initiator (ammonium persulfate, APS, 3% w/v). The initiator was located in the middle fluid, whereas the accelerator was dissolved in the inner oil. The molar ratio of METAC to NIPAM was 5.6%. The middle fluid (MF) for the batch 2 sample was the same as that for batch 1 except that it contained less cross-linker (0.64% w/v BIS) and did not contain METAC, which provided positive charges to the gel shell (batch 1).

Upon the formation of the double emulsion drops, the accelrator diffused from the internal oil droplet into the surrounding aqueous monomer solution layer, initiating the polymerization. We matched the density of the water phase to 1.05 g·mL^{-1} by mixing glycerol (10 vol %) and deuterium oxide

(22 vol %). The flow rate (Q) conditions were Q_{IF} = 100 μL·h^{-1}, Q_{IF} = 300 μL·h^{-1}, and Q_{IF} = 2000 μL·h^{-1}. By tuning the flow rates of the three fluid streams, we were able to produce microgel particles at rates of ~10^3 Hz. After we collected the particles, they were washed repeatedly with large amounts of isopropyl alcohol, which removed the silicon oil and were transferred to deionized water. Swelling measurements were carried out in water. Figure 2b shows the formation of premicrogel double emulsion drops. Uniform microgel shells were obtained after solidifying the emulsion by the redox reaction (Figure 2c). It is noted that when the inner and outer oils of the shells in Figure 2b,c were removed and the shells were placed in

water, the sizes of the shells should approximately double because of the hydrophilic nature of the polymer network.

3b. Observation of the Volume Phase Transition and Swelling Kinetics. The volume phase transition of the microgel shells was monitored by the use of a bright field microscope (Leica) equipped with a digital camera (Hamamatsu, C4742-95) and Simple PCI acquisition software (Compix). For this, we completely sealed the microgel shells in flat glass capillaries (inner diameters ∼300 μm, VitroCom). Figure 3 shows temperature-dependent inner (●) and outer (■) radii for sample batch 1 in water. The sharp volume change at ∼44 °C is determined to be the transition temperature. This temperature is >34 °C for neutral PNIPAM gel because of the incorporation of ionic groups from MATEC into the polymer network.

The PNIPAM microgel shells in pure water were put in a transparent holder on a glass slide, which was placed on a microscope-mounted heating and cooling stage (Physitemp Instruments, TS-4ER) to examine the thermosensitive behavior. Several microgel shells with the same structures were measured to obtain data with better statistics for the thermoresponsive characteristics. The temperature of the liquid inside the sample holder was confirmed using an infrared thermometer (VWR).[26]

4. Results and Discussion

4a. Basic Theoretical Calculations. In Figure 4, we show an arbitrary solution to the radial displacement vector $u(r,t)$ at various times as calculated by our model. The solution is calculated up to the tenth order, and the parameters are selected to be $a = 2$, $b = 1$, and $\Delta a = 2$. Each of the curves is plotted as a function of the radius in the interval $b < r < a$. The times have been normalized to the first-order time constant in eq 13, $\tau = 1/(D_0\lambda_1^2)$. At the initial time $t/\tau = 0$,

the displacement $u(r,t)$ is expressed as a nearly straight line as a function of r. The wiggles are caused by the finite number of terms in the series in eq 13. As t/τ increases, the wiggles disappear because the higher order terms are dying off exponentially.

Figure 5 shows a set of curves for the radial component of the stress tensor $\sigma_{rr}(r,t)$, which is calculated by taking the solution eq 13 and applying the differential operator described by eq 4. Because differentiation emphasizes any nonmonotonic features, the oscillations in Figure 5 are more pronounced as compared with those in Figure 4. We used the same values for a, b, and Δa as in Figure 4, and $K = 1$ for the bulk modulus. According to the initial condition eq 5, swelling starts from uniform radial stress $\sigma_{rr}(r,t = 0) = (3K\Delta a)/a$, whereas the eigenfunctions $Z_n(r)$ satisfy the stress-free boundary condition eq 4. A transition from uniform stress to zero stress occurs in the very initial stage of the evolution when the acceleration term cannot be neglected in eq 1. The length of this transient stage depends on the liquid viscosity, and it is usually very short as compared with the typical relaxation time, τ. Because we neglect the length of the transient stage, the numerical curve $t = 0$ in Figure 5 obtained for a finite number of terms $n = 10$ tends to zero near the inner surface $r = b$.

Li and Tanaka found the isotropic condition $u_r/r = u_z/z$ for a thin disk or a long cylinder gel, where u_r/r and u_z/z are the relative swelling along the radial and longitudinal directions, respectively.[15] By minimizing shear elastic energy, we obtain the boundary condition, eq 12. At $t/\tau \to \infty$, the radial stress $\sigma_{rr} \to 0$ at both $r = a$ and $r = b$ and the isotropic condition $u(a,\infty)/a = u(b,\infty)/b$ is satisfied, as expected.
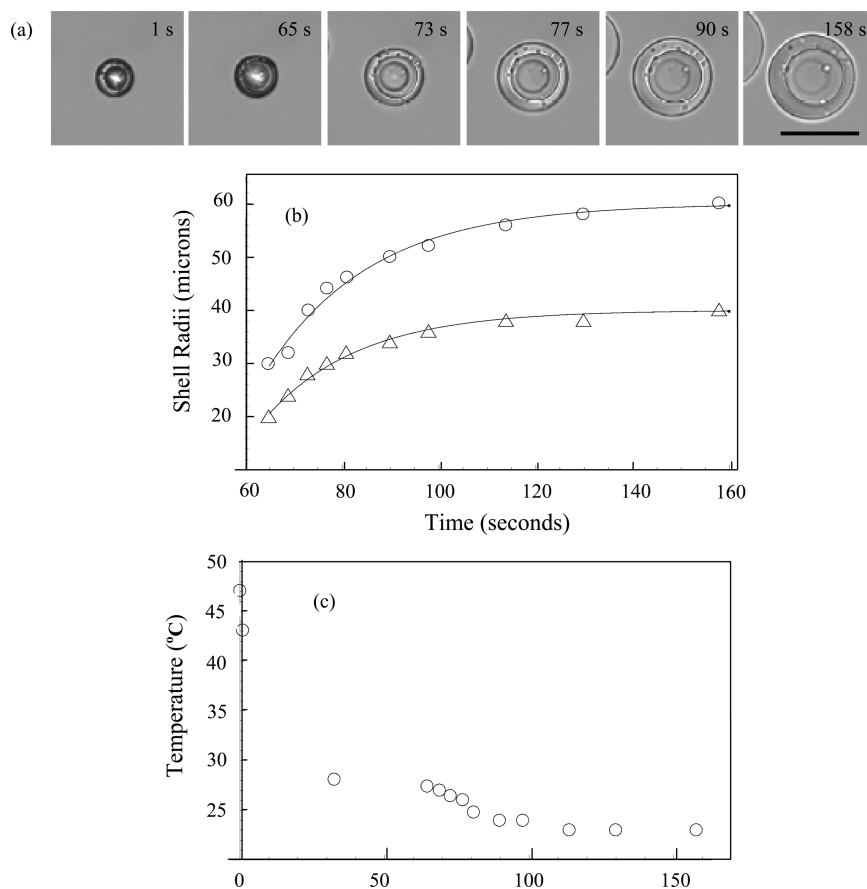

Figure 7. (a) Progress of swelling for the neutral microgel shell (batch 2) as the temperature jump was taken from 47 to 23 °C. Scale bar = 100 μm. (b) Graph shows the inner (△) and outer (○) radii of the gel shell radii versus elapsed time for a swelling process. The solid curves are calculated by our model. (c) Temperature for the sample holder of this experiment versus time.
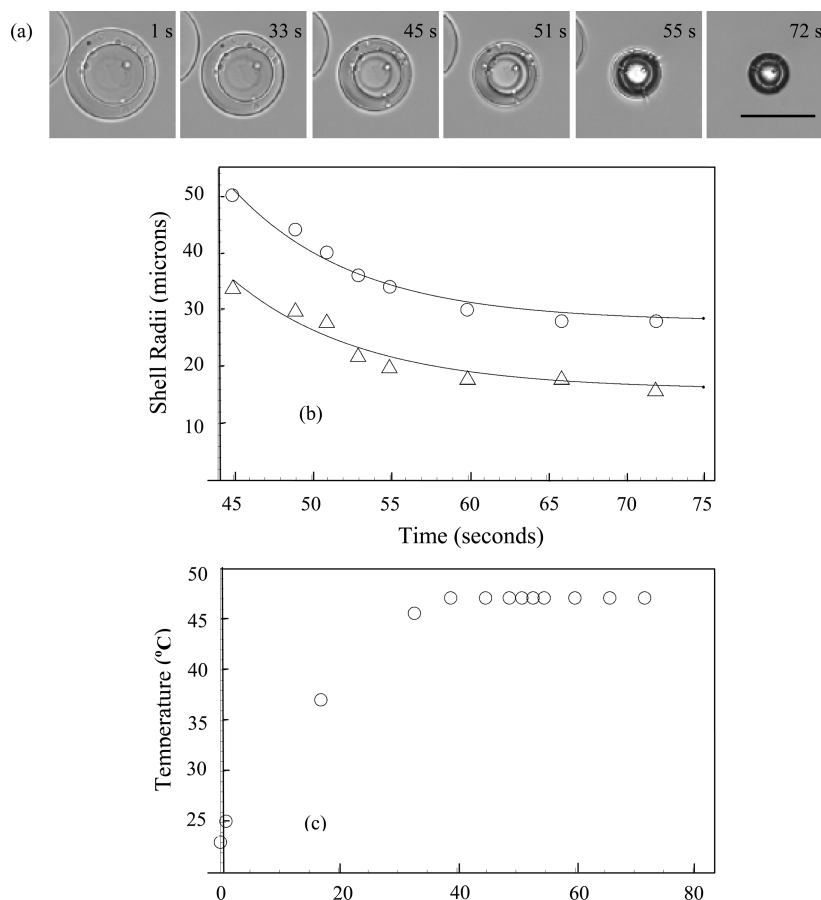
Figure 8. (a) Progress of shrinking for the neutral microgel shell (batch 2) as the temperature jump was taken from 23 to 47 °C. Scale bar = $100 \mu m$. (b) Graph shows the inner ($\triangle$) and outer ($\bigcirc$) radii of the gel shell radii versus elapsed time for a shrinking process. The solid curves are calculated by our model. (c) The temperature for the sample holder of this experiment versus time.

4b. Comparison with Experimental Data. A typical series of photos of shrinking kinetics for an ionic microgel shell (batch 1) is shown in Figure 6a. The experimental data for outer ($\bigcirc$) and inner ($\triangle$) radii are plotted in Figure 6b. Solid lines represent the evolution obtained for the outer radius $\mathscr{R}(r = a,t) = a + u(a,t)$ and the inner radius $\mathscr{R}(b,t) = u(b,t)$ of the swelling ($u < 0$) or shrinking ($u > 0$) shell. To plot the displacements $u(a,t)$ and $u(b,t)$, we keep only the first term ($n = 1$) in eq 13, that is

$$\mathscr{R}(r, t) = r \pm \sum_{n=1}^{\infty} A_n Z_n(r) e^{-\lambda_n^2 D_0 t} \cong r \pm A_1 Z_1(r) e^{-t/\tau} \quad (36)$$

This approximation is valid at $t > \tau$ when the terms with $n > 1$ are exponentially small.

We present a further comparison of swelling and shrinking results for a neutral microgel shell (batch 2) that appear in Figures 7 and 8. Notice that some of the shells analyzed in this study have a noticeable asymmetry. (See Figure 7a.) Because there is a good agreement between the theory and experiment, we may assume that this slight asymmetry does not have much effect on the evolution of the gel shells.

For each of the fits performed here, we begin by identifying the necessary parameters from the experiment: the equilibrium shell radii (a and b) and the total change of the outer radius, Δa. These parameters are then substituted into eq 36. A nonlinear fit is employed to find the appropriate value for the collective diffusion coefficient, D_0. The starting time for the solution is selected on the basis of the temperature measurements within the sample holder. We can see from the temperature curves in Figures 7c and 8c that the

change of temperature within the sample holder occurs on a time scale that is comparable to that of the swelling (or shrinking) time scales. In the ideal situation, this comparison is done such that the heating time for the sample holder is much smaller than that of the swelling time. Because the diffusion coefficient is temperature dependent, the start time must be selected appropriately to ensure that the fit is done within the time scale where the temperature gradient is negligible. Start times are selected by inspection of the data and are chosen by the point where the temperature stabilizes.

Using the data shown in Figure 6, we have found the collective diffusion coefficient $D_0 = 5.7 \times 10^{-8} \text{ cm}^2 \cdot \text{s}^{-1}$ for the shrinking experiment for the ionic microgel shell (batch 1) at 60 °C in Figure 6. The shrinking kinetics for submillimeter ionic solid gel spheres have been previously studied with three characteristic processes: initially the gel shrinks and maintains its spherical shape, then the shrinking stops (known as a plateau period), and finally bubbles appear on the surface of the gel.[28] As shown in Figure 6a, our shell uniformly shrank from the beginning to the end without the development of the transient surface pattern. This suggests that for a very small gel such as a microgel shell there appears no mechanical instability due to a large volume change in the shrinking process that can cause surface patterns.

For the neutral microgel shell (batch 2), we found that $D_0 = 2.0 \times 10^{-7} \text{ cm}^2 \cdot \text{s}^{-1}$ for swelling at 23 °C (Figure 7) and $D_0 = 1.1 \times 10^{-7} \text{ cm}^2 \cdot \text{s}^{-1}$ for shrinking at 47 °C (Figure 8). These values are in excellent agreement with the previous measurements made for neutral PNIPAM submillimeter solid gel spheres that did not have a transient surface pattern during shrinking at each of the respective temperatures.
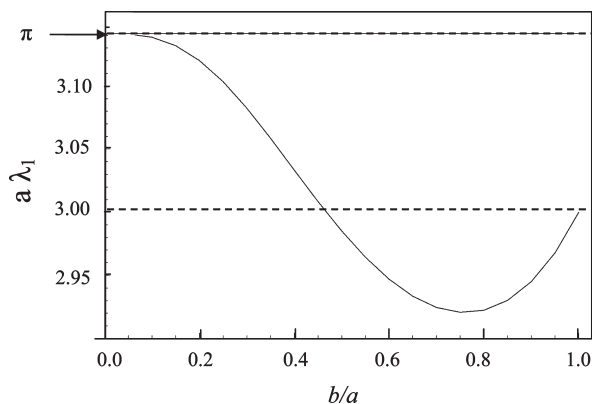
Figure 9. First eigenvalue solution to eq 16 plotted as $a\lambda_1$ versus the ratio (b/a) of the inner radius (b) to the outer radius (a). The dashed lines show two limiting cases: as $b \to 0$ (a solid sphere), $\lambda_1 \to \pi$; as $b \to a$ (a balloon), $a\lambda_1 \to 3$.
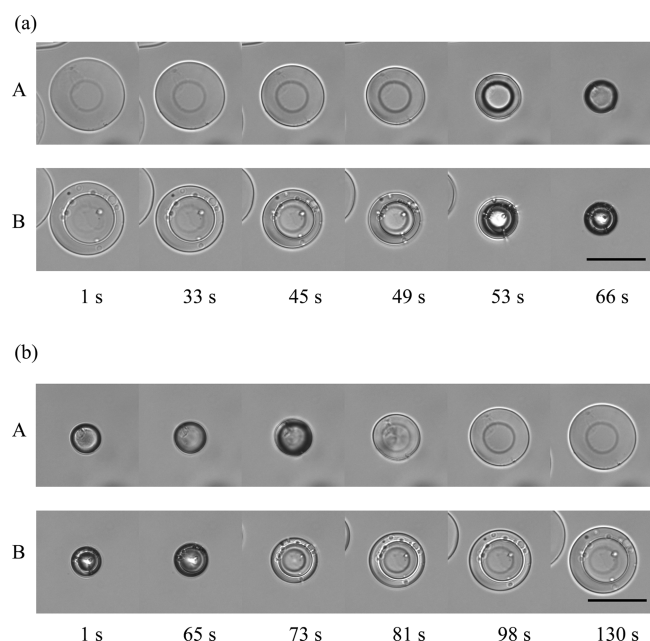
(a)

(b)

Figure 10. Comparison of swelling kinetics between a solid microgel (A) and a microgel shell (B) upon (a) heating from 23 to 47 °C and (b) cooling from 47 to 23 °C. Scale bar = 100 μm.

These previous measurements showed that $D_0 = 2.0 \times 10^{-7}$ cm$^2\cdot$s^{-1} at 23 °C and $D_0 = 1.6 \times 10^{-7}$ cm$^2\cdot$s^{-1} at 47 °C.[29]

4c. Comparison of a Solid Sphere with a Shell. For a diffusion process, the time required for matter to diffuse at some distance changes quadratically with the distance. In particular, the solution obtained for a solid sphere gives[11]

$$\tau \propto a^2/D_0 \qquad (37)$$

For a shell, one can expect that $\tau_{shell} \propto (a-b)^2$. However, our results show that $\tau_{shell} \propto a^2$. That is, the characteristic time of a gel shell should be proportional to the square of the outer radius, not to the squared thickness of the shell. Indeed, for a thin shell (balloon) when $(a-b) \to 0$, the characteristic time remains finite, and according to eq 35

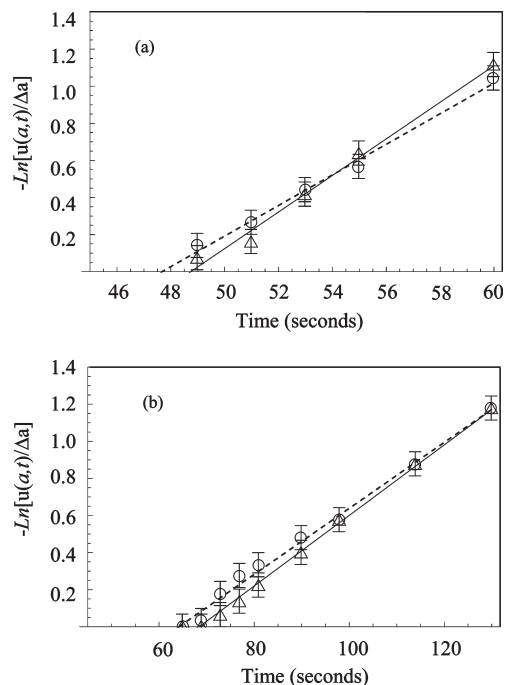$$\tau_{shell} = \frac{1}{\lambda^2 D_0} = \frac{a^2}{9D_0} \qquad (38)$$

Figure 11. Comparison of the relative displacements for the solid microgel sphere ($\triangle$) and the microgel shell ($\bigcirc$) as a function of time: for the (a) shrinking and (b) swelling processes, respectively.

For a solid sphere ($b = 0$), the characteristic time is given by the lowest eigenvalue in the spectrum eq 7, $\lambda_1 = \pi/a$

$$\tau_{solid} = \frac{1}{\lambda_1^2 D_0} = \frac{a^2}{\pi^2 D_0} \qquad (39)$$

For the intermediate case, when $0 < a - b < a$ the lowest eigenvalue λ_1 obtained from eq 16 lies between $2.9/a$ and π/a, as plotted in Figure 9. Because the relative variation of λ_1 versus $a - b$ does not exceed 4%, we may conclude that for a shell the characteristic time is approximately proportional to a^2. We suggest that the relationship of $\tau \propto a^2$ is caused by the constraint imposed at the inner boundary eq 12. In contrast with the outer shell, which is always stress-free, there is a large increase in the stress at the inner surface soon after the shell starts to swell. This stress constrains the gel shell to swell slower for the readjustment of shape necessary to minimize the shear energy integral eq 10.

From the plot in Figure 9 and the relation $\tau \propto 1/\lambda_1^2$, one can conclude that the solid sphere swells a bit faster than a shell. However, the difference in the characteristic times is less than $0.01a^2/D_0$. Such a small difference is hard to detect experimentally.

To investigate the above results further, we have reexamined the swelling and shrinking kinetics data that were published in ref 26 and adapted in Figure 10. Here swelling (Figure 10a) and shrinking kinetics (Figure 10b) between a solid microgel (series A) and a gel shell (series B) are compared. There is no discernible difference between the solid sphere and a gel shell just by visual inspection.

A comparison of the relative displacements for the sphere and the shell as a function of time are shown in Figure 11. As an approximation, we have used the first time exponential term $e^{-t/\tau}$ to fit both curves. We find that the values of τ in the shrinking process are 10.1 ± 1.2 and 12.2 ± 1.2 s for the solid sphere and the shell, respectively, as shown in Figure 11a. In the case of swelling (Figure 11b), the characteristic times are calculated to be 52 ± 2 and 56 ± 4 s for the solid sphere and

shell, respectively. These characteristic times are very close to one another. It may appear that the shell swells slower than the solid sphere, but with the experimental error taken into account, we cannot conclude any quantitative difference between the two.

5. Conclusions

We have built a theoretical model for the swelling kinetics of a polymer gel shell by considering the shell with outer and inner radii a and b, respectively. For the outer layer, there is the same free surface boundary condition as that for a solid gel sphere. The boundary condition at the inner surface is obtained from the minimization of shear elastic energy. We solved the diffusion equation for the displacement vector $u(r,t)$ with two boundary conditions and with the initial condition of uniform stress at $t = 0$. Our results recover the solution to Tanaka and Fillmore's solid sphere solution as $b \rightarrow 0$. In the opposite limiting case, $b \rightarrow a$, we find that the swelling of a thin shell like a balloon is described simply by a single exponential term.

To test our theoretical model, we have made monodisperse PNIPAM polymer gel shells using a microfluidic device. These gels typically have an inner radius of $\sim$40 μm and an outer radius of $\sim$60 μm. By switching temperatures, we have measured the inner and outer radii of the shell as a function of time and have found the collective diffusion coefficient for the shrinking experiment for the ionic microgel shell (batch 1) at 60 °C to be $D_0 = 5.7 \times 10^{-8}$ cm$^2 \cdot$s^{-1}. The shell uniformly shrank from the beginning to the end without the development of the transient surface pattern. For the neutral microgel shell (batch 2), the diffusion coefficients are found to be $D_0 = 2.0 \times 10^{-7}$ cm$^2 \cdot$s^{-1} for swelling at 23 °C and $D_0 = 1.1 \times 10^{-7}$ cm$^2 \cdot$s^{-1} for shrinking at 47 °C. These values are in agreement with the previous measurements made for neutral PNIPAM submillimeter solid gel spheres at each of the respective temperatures: $D_0 = 2.0 \times 10^{-7}$ cm$^2 \cdot$s^{-1} at 23 °C and $D_0 = 1.6 \times 10^{-7}$ cm$^2 \cdot$s^{-1} at 47 °C.[29]

Our model shows that the characteristic time of a gel shell is proportional to the square of the outer radius, not to the square of the thickness of the shell. This is because both boundaries are coupled via the boundary condition that originates from the minimization of shear elastic energy. This conclusion is confirmed by experimental observation of swelling kinetics. Our model further predicts that the solid sphere swells slightly faster than the gel shell if they have the same outer radius. The experiments nearly confirm this tendency, although the lack of experimental accuracy does not allow for a reasonable quantitative comparison.

References and Notes

(1) Peppas, N. A. *Hydrogels in Medicine and Pharmacy*; CRC Press: Boca Raton, FL, 1987.
(2) Hoffman, A. S. *J. Controlled Release* **1987**, *6*, 297.
(3) Li, Y.; Tanaka, T. *Annu. Rev. Mater. Sci.* **1992**, *22*, 243.
(4) Siegel, R. *Adv. Polym. Sci.* **1993**, *109*, 233.
(5) Shibayama, M.; Tanaka, T. *Adv. Polym. Sci.* **1993**, *109*, 1.
(6) Gehrke, S. H. *Adv. Polym. Sci.* **1993**, *110*, 81.
(7) Hu, Z.; Zhang, X.; Li, Y. *Science* **1995**, *269*, 525.
(8) Osada, Y.; Gong, J. P. *Adv. Mater.* **1999**, *10*, 827.
(9) Flory, P. J.; Rehner, J. *J. Chem. Phys.* **1943**, *11*, 521.
(10) Ritger, P. L.; Peppas, N. A. *J. Controlled Release* **1987**, *5*, 37.
(11) Tanaka, T.; Fillmore, D. J. *J. Chem. Phys.* **1979**, *70*, 1214.
(12) Tanaka, T.; Hocker, L. O.; Benedek, G. B. *J. Chem. Phys.* **1973**, *59*, 5151.
(13) Peters, A.; Candau, S. J. *Macromolecules* **1986**, *19*, 1952.
(14) Peters, A.; Candau, S. J. *Macromolecules* **1988**, *21*, 2278.
(15) Li, Y.; Tanaka, T. *J. Chem. Phys.* **1990**, *92*, 1365.
(16) Wang, C. J.; Li, Y.; Hu, Z. B. *Macromolecules* **1997**, *30*, 4727.
(17) Urayama, K.; Okada, S.; Nosaka, S.; Watanabe, H.; Takigawa, T. *J. Chem. Phys.* **2005**, *122*, 024906.
(18) Yamaue, T.; Doi, M. *J. Chem. Phys.* **2005**, *122*, 084703.
(19) Doi, M. *J. Phys. Soc. Jpn.* **2009**, *78*, 052001.
(20) Birgersson, E.; Li, H.; Wu, S. *J. Mech. Phys. Solids* **2008**, *56*, 444.
(21) Ichikawa, H.; Fukumori, Y. *J. Controlled Release* **2000**, *63*, 107.
(22) Koh, W. G.; Revzin, A.; Pishko, M. V. *Langmuir* **2002**, *18*, 2459.
(23) Gu, J.; Xia, F.; Wu, Y.; Qu, X.; Yang, Z.; Jiang, L. *J. Controlled Release* **2007**, *117*, 396.
(24) Lawrence, D. B.; Cai, T.; Hu, Z.; Marquez, M.; Dinsmore, A. D. *Langmuir* **2007**, *23*, 395.
(25) Kim, J.-W.; Utada, A. S.; Fernandez-Nieves, A.; Hu, Z. B.; Weitz, D. A. *Angew. Chem., Int. Ed.* **2007**, *46*, 1819–22.
(26) Chu, L.-Y.; Kim, J.-W.; Shah, R. K.; Weitz, D. A. *Adv. Funct. Mater.* **2007**, *17*, 3499–3504.
(27) Trefethen, L. N.; Bau, D., III. *Numerical Linear Algebra*; Society for Industrial and Applied Mathematics: Philadelphia, PA, 1997.
(28) Sato Matsuo, E.; Tanaka, T. *J. Chem. Phys.* **1988**, *89*, 1965–1703.
(29) Tanaka, T.; Sato Matsuo, E.; Hirokawa, Y.; Hirotsu, S.; Peetermans, J. *Phys. Rev. Lett.* **1985**, *55*, 2455–2458.